Soft Matter

Accepted Manuscript

ROYAL SOCIETY OF CHEMISTRY

www.rsc.org/softmatter

Table of Contents Entry

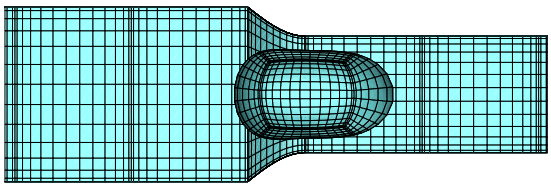

Based on computational modeling, we develop a new methodology to determine a membrane's shear modulus, independently of its area-dilatation modulus, via capsule flow in a converging microcapillary.

Determining a membrane's shear modulus, independently of its area-dilatation modulus, via capsule flow in a converging micro-capillary

P. Dimitrakopoulos* and S. Kuriakose
Department of Chemical and Biomolecular Engineering, University of Maryland, College Park, Maryland 20742, USA
(Dated: February 2, 2015)

The determination of the elastic properties of the membrane of artificial capsules is essential for the better design of the various devices that are utilized in their engineering and biomedical applications. However this task is complicated owing to the combined effects of the shear and area-dilatation moduli on the capsule deformation. Based on computational investigation, we propose a new methodology to determine a membrane's shear modulus, independently of its area-dilatation modulus, by flowing strain-hardening capsules in a converging micro-capillary of comparable size under Stokes flow conditions, and comparing the experimental measurements of the capsule elongation overshooting with computation data. The capsule prestress, if any, can also be determined with the same methodology. The elongation overshooting is practically independent of the viscosity ratio for low and moderate viscosity ratios, and thus a wide range of capsule fluids can be employed. Our proposed experimental device can be readily produced via glass fabrication while owing to the continuous flow in the micro-capillary, it is possible the characterization of a large number of artificial capsules.

1. INTRODUCTION

The study of the interfacial dynamics of artificial or physiological capsules (i.e. membrane-enclosed fluid volumes) in viscous flows has seen an increased interest during the last few decades owing to their numerous engineering and biomedical applications [29, 41]. In the area of interest of the present paper, the study of the motion and deformation of capsules and biological cells in micro-channels is motivated by a wide range of applications including drug delivery, cell sorting and cell characterization devices [1, 6], fabrication of microparticles and microcapsules with desirable properties [7, 33], determination of membrane properties [22, 30], and of course its similarity to blood flow in vascular capillaries [31, 39].

The determination of the elastic properties of the membrane of artificial capsules (i.e. the shear modulus G_s and area-dilatation modulus G_a) is essential for the better design of the various devices that are utilized [21, 22]. For this, several techniques have been developed including static compression and shear, extensional or centrifugal flow fields for milli-capsules [3–5, 28] as well as micropipette and atomic force microscope measurements, and flow in microfluidic channels and tubes for microcapsules, e.g. [9, 21–23, 26, 30]. We emphasize that the mechanical determination of membranes is a challenging task (especially for micro-capsules), while two experimental techniques are commonly required to account for the combined effects of the shear and area-dilatation moduli on the membrane deformation [21, 28].

In our recent paper [10], we proposed a new methodology to identify the shear and area-dilatation moduli of individual milli- and micro-capsules, by comparing our computation data with experimental measurements of two capsule dimensions at moderate and strong planar extensional flows in classical or microfluidic "four-roll mill" devices. This procedure has the advantage of not depending on, or being influenced by, the fluids viscosity ratio because, owing to the specific symmetry of the planar extensional flow, at steady state there is no flow inside the capsule, as also happens for steady-state capsule motion in solid ducts [10, 19, 20, 23, 32].

Therefore, the membrane moduli determination relies on capsule dynamics, including deformation and motion, under transient or steady-state conditions, which is complicated owing to the nonlinear coupling of the deforming hydrodynamic forces with the restoring interfacial forces of the capsule membrane. Thus, the capsule dynamics is affected in general by several parameters, including the capillary number (i.e. the ratio of the deforming viscous stresses to restoring shearing stresses on the membrane), the fluids viscosity ratio for transient dynamics, capsule prestress (if any), the moduli ratio G_a/G_s, and the degree of strain-hardening or strain-softening of the membrane (i.e. the membrane nature) for non-linear capsule dynamics. In transient conditions, the effects of the fluids viscosity ratio can be eliminated by employing very viscous surrounding fluids which makes the capsule dynamics independent of the (exact value of the) viscosity of the capsule fluid [22, 27].

However, under any conditions, the local tensions and deformation of a membrane result from the combined effects of two basic types of deformations, i.e. shearing in-plane without changing surface area (associated with G_s) and extended in-plane such that the surface area increases (associated with G_a). As a consequence, the moduli determination of a capsule is a challenging task, requiring the measurement of at least two independent

* dimitrak@umd.edu

capsule properties, commonly via two experimental techniques or via one experimental technique involving measurement of different capsule properties, to account for the combined effects of both membrane moduli on the capsule dynamics [10, 21, 28]. It is of interest to note that even the determination of the shear modulus alone still requires the measurement of at least two independent capsule properties (or the *a priori* knowledge of, or assumption on, the value of the moduli ratio G_a/G_s) since, in general, both membrane moduli affect the capsule dynamics [8, 18, 21, 24].

In addition, without the *a priori* knowledge of the moduli ratio G_a/G_s (as it is the case for a new or unknown membrane), the determination of a membrane's shear modulus G_s requires significant testing to verify the correct value of the moduli ratio G_a/G_s, for all techniques involving both linear or nonlinear capsule deformations. This task is more complicated for experimental techniques involving three-dimensional capsule deformation (e.g. flow in microfluidic channels) since the required for comparison three-dimensional computational data may be difficult to obtain for a wide rage of G_a/G_s. (For methodologies involving nonlinear capsule deformations, the strain-hardening (or strain-softening) nature of the membrane also affects the capsule dynamics, and thus additional testing may be necessary, e.g. by utilizing different constitutive laws to describe the membrane tensions [18].) On the other hand, assumption of the moduli ratio G_a/G_s may simplify the modulus determination [24], but there is no guarantee that the derived modulus value represents the true shear modulus of the membrane.

Based on computational investigation, in this paper we develop a new methodology to determine a membrane's shear modulus G_s, independently of its area-dilatation modulus G_a, by flowing strain-hardening capsules in a converging micro-capillary of comparable size under Stokes flow conditions, and comparing the experimental measurements of the capsule elongation overshooting with computation data. The capsule prestress, if any, can also be determined with the same methodology. The elongation overshooting is practically independent of the viscosity ratio for low and moderate viscosity ratios, and thus a wide range of capsule fluids can be employed. Our proposed experimental device can be readily produced via glass fabrication while owing to the continuous flow in the micro-capillary, it is possible the characterization of a large number of artificial capsules. After the shear modulus determination, the area-dilatation modulus G_a of the membrane can easily be determined via any existing methodology, e.g. steady-state motion in a microchannel. To the best of our knowledge, this is the first methodology which can determine a membrane's shear modulus independently of its area-dilatation modulus for an array of capsules.

2. PROBLEM DESCRIPTION

We consider a three-dimensional capsule (i.e. a fluid volume enclosed by a thin elastic membrane) with a spherical undisturbed shape. The capsule is flowing along the centerline of a straight micro-channel with a converging section in the middle connecting two square channels, as shown in figure 1. We emphasize that the centerline requirement is not a restriction for our study since this is the steady-state location of spherical capsules in a square channel [19]; thus our capsules are expected to have been aligned with the micro-capillary centerline during their motion in the area further upstream the constriction.

To facilitate our description, we imagine that the channel is horizontal as illustrated in figure $1(a)$. Thus, the flow direction (i.e. the x-axis) corresponds to the channel's or capsule's length, the z-direction will be referred as height while the y-direction will be referred as width. The height of the square micro-channel at the left is $3\ell_z$ and that of the square micro-channel at the right $2\ell_z$. The converging middle section, which connects the two square micro-channels, has length $\ell_{con} = \ell_z$. Each of the two square micro-channels has length $12\ell_z$, and thus the length of the entire microfluidic device is $25\ell_z$. The half-height ℓ_z of the downstream square micro-channel serves as the length scale for the present problem while the origin of the co-ordinate system is placed at the beginning of this channel (just after the converging middle section) as shown in figure $1(a)$.

The shape of the converging middle section in our micro-geometry is defined by a "quarter-cosine" variation, which for the co-ordinate system shown in figure $1(a)$ is given by

$$f(x) = \ell_z\Big\{\frac{3}{2} + \frac{1}{2}\cos\Big[(\frac{x}{\ell_z} + 2)\frac{\pi}{2}\Big]\Big\} \tag{1}$$

where $-1 \leq x/\ell_z \leq 0$ and $f(x)$ defines the geometry's height $z(x)$ or width $y(x)$. It is of interest to mention that, although the results presented in this paper were derived utilizing this shape of the converging middle section, we derived very similar (or practically identical) results utilizing other converging shapes, including "half-cosine" variation

$$f(x) = \ell_z\Big\{\frac{5}{4} + \frac{1}{4}\cos\Big[(\frac{x}{\ell_z} - 1)\pi\Big]\Big\} \tag{2}$$

and "straight-line" connection

$$f(x) = \ell_z\Big(1 - \frac{1}{2}\frac{x}{\ell_z}\Big) \tag{3}$$

Similar devices involving converging micro-capillaries with circular or square cross-sections have been produced via glass fabrication to study soft particles, e.g. for the generation of monodisperse double emulsions and the elasticity determination of soft gels [14, 34, 35].

The capsule's interior and exterior are Newtonian fluids, with viscosities $\lambda\mu$ and μ, and the same density. The

capsule size a is specified by its volume $V = 4\pi a^3/3$ and is comparable to the micro-geometry's half-height ℓ_z. In addition, we consider that the capsule is slightly over-inflated, made of a strain-hardening membrane following the Skalak *et al.* constitutive law [36] (and thus called Skalak capsule in this paper) with comparable shearing and area-dilatation resistance. This capsule description represents well bioartificial capsules such as the capsules made of covalently linked human serum albumin (HSA) and alginate used in the experimental study of Risso, Collé-Pailot and Zagzoule [32].

Our membrane description is based on the well-established continuum approach and the theory of thin shells by considering the membrane as a two-dimensional continuum with shearing and area-dilatation resistance but negligible bending resistance. This modeling has been proven to be an excellent description of a wide range of thin elastic membranes (such as biocompatible alginate, synthetic polysiloxane and aminomethacrylate capsules) whose thickness is several orders of magnitude smaller than the size of the capsules (up to a membrane thickness of 5% the capsule size), and their bending resistance is very small compared to their shearing resistance [3, 11, 13, 23, 28].

The surface stress is determined by the in-plane stresses

$$\Delta \boldsymbol{f} = -\nabla_s \cdot \boldsymbol{\tau} = -(\tau^{\alpha\beta}|_\alpha \, \boldsymbol{t}_\beta + b_{\alpha\beta}\, \tau^{\alpha\beta}\, \boldsymbol{n}) \qquad (4)$$

where the Greek indices range over 1 and 2, while Einstein notation is employed for (every two) repeated indices. In this equation, the $\tau^{\alpha\beta}|_\alpha$ notation denotes covariant differentiation, $\boldsymbol{t}_\beta = \partial \boldsymbol{x}/\partial\theta^\beta$ are the tangent vectors on the capsule surface described with arbitrary curvilinear coordinates θ^β, and $b_{\alpha\beta}$ is the surface curvature tensor [12, 29]. The in-plane stress tensor $\boldsymbol{\tau}$ is described by the strain-hardening constitutive law of Skalak *et al.* [36] which relates $\boldsymbol{\tau}$'s eigenvalues (or principal elastic tensions $\tau^P_\beta, \beta = 1, 2$) with the principal stretch ratios λ_β by

$$\tau^P_1 = \frac{G_s \lambda_1}{\lambda_2}\{\lambda_1^2 - 1 + C\lambda_2^2[(\lambda_1\lambda_2)^2 - 1]\} \qquad (5)$$

Note that the reference shape of the elastic tensions is the spherical quiescent shape of the capsule while to calculate τ^P_2 reverse the λ_β subscripts. In Eq.(5), G_s is the membrane's shear modulus while the dimensionless parameter C describes the membrane hardness (i.e. the strength of its strain-hardening nature) and is associated with the scaled area-dilatation modulus G_a of the membrane, $G_a/G_s = 1 + 2C$ [29, 36].

To quantify the capsule over-inflation, we define the prestress parameter α_p such that all lengths in the undeformed capsule would be scaled by $(1 + \alpha_p)$ relatively to the reference shape [19, 20, 27]. Since the capsule is initially spherical, its membrane is initially prestressed by an isotropic elastic tension $\tau_0 = \tau^P_\beta(t = 0)$ which depends on the employed constitutive law and its parameters but not on the capsule size. For example, for a Skalak capsule with $C = 1$ and $\alpha_p = 0.05$, the undisturbed capsule radius a is 5% higher than that of the reference shape and the initial membrane tension owing to prestress is $\tau_0/G_s \approx 0.3401$. In addition, incorporation of prestress into our elastic membrane model removes the buckling instability observed in axisymmetric-like flows. (See section 2 in Ref.[19].)

At time $t = 0$ the capsule is located at $-5\ell_z$ on the micro-channel centerline, the flow is turn on inside the microfluidic device and we investigate the transient dynamics of the capsule as it enters and exits the constriction which occupies the x-region $[-\ell_z, 0]$. (The specific choice for the capsule's initial position does not affect the capsule deformation and motion inside the constriction or downstream of it, i.e. we obtained identical results even for capsules placed further upstream the constriction.)

At the micro-capillary ends the flow approaches the undisturbed flow $\boldsymbol{u}^\infty$ in a square channel which serves as the boundary condition assuming a fixed flow rate Q inside the micro-device. (The exact form of the channel's velocity field $\boldsymbol{u}^\infty$ and its average velocity $\mathcal{U}$ are given in section 2 of our earlier paper on capsule motion in a square micro-channel [19].) We assume that the Reynolds number is small for both the surrounding and the inner flows, and thus the capsule deformation occurs in the Stokes regime.

The numerical solution of the interfacial problem is achieved through our interfacial spectral boundary element method for membranes [12] which has been employed for the study of the capsule dynamics in square and rectangular microfluidic channels [19, 20, 27]. For more details on our capsule modeling and the computational method, the interested reader is referred to section 2 of our earlier papers [12, 19] as well as the electronic supplementary information of this paper. To verify the accuracy of our results, we performed convergence runs covering the entire interfacial evolution with different spacial grids for several capsules and flow rates. Our convergence runs showed that our results for the interfacial shape, the capsule velocity and the additional pressure difference presented in this work were determined with an accuracy of at least 3 significant digits.

In our work, we consider Skalak capsules with different size a/ℓ_z, membrane hardness C and prestress α_p. The present problem depends on two additional dimensionless parameters, the fluids viscosity ratio λ and the capillary number Ca defined as

$$\mathrm{Ca} = \frac{\mu \mathcal{U}}{G_s} \qquad (6)$$

where $\mathcal{U}$ is the average undisturbed velocity at the downstream square micro-channel. It is of interest to note that the capillary number, as defined by Eq.(6), does not contain any length scale, and thus it may be considered as a dimensionless flow rate. Note that we investigate capsules with size $a/\ell_z = 0.6$–1.3, hardness $C = 0.1$–5, prestress $\alpha_p = 0.01$–0.1, and viscosity ratio $\lambda = 0.01$-10, in flows with capillary number $\mathrm{Ca} = 0.02$–0.3. This range of dimensionless parameters can readily be used in experimental microfluidic systems, e.g. see [18, 22, 23, 32]. In

our study, the velocity is scaled with the average undisturbed velocity $\mathcal{U}$ and the pressure with the associated pressure scale, $\Pi = \mu\mathcal{U}/(2\ell_z)$, in the downstream square channel.

3. CAPSULE DYNAMICS IN A CONVERGING MICRO-CHANNEL

The transient deformation of a capsule moving though the converging micro-channel is shown in figure 2. At the upstream square channel, the capsule obtains a spherical-like shape with a pointed downstream edge, as seen in figure 2(a), because the local surrounding flow is not strong enough the cause a significant capsule deformation owing to the larger cross-section of the upstream channel. The capsule shape becomes more deformed and pointed as the capsule enters the constriction, shown in figure 2(b), owing to the strong hydrodynamic forces associated with the local cross-sectional area decrease which gradually increases the average fluid velocity inside the constriction since the flow rate Q is fixed in our problem. To balance the deforming hydrodynamic forces, the capsule tries to increase its downstream curvature and decrease its upstream curvature so that the total restoring tension force on the membrane is increased. In essence, this capsule deformation results from the curvature term in the membrane traction, Eq.(4), as we identified in our earlier studies on capsule dynamics in square or rectangular microfluidic channels [19, 20, 27]. As the capsule moves out of the constriction and into the smaller square channel at the right, the capsule elongates while its shape becomes cylindrical-like, as seen in figure 2(c). Finally at the downstream square channel, the capsule obtains the typical axisymmetric-like bullet shape, shown in figure 2(d), owing to the stronger confinement and thus the stronger local hydrodynamic forces [18, 19, 22, 32].

In essence, the specific micro-geometry employed in this work, connects via the converging constriction, the two capsule regimes identified in our earlier work on the steady-state capsule motion in axisymmetric-like, square or cylindrical, channels [19].

In particular, for small and moderate capsule sizes (i.e. $a/\ell_z \lesssim 0.8$), our earlier investigation [19] revealed that the capsule velocity U_x and additional pressure drop ΔP^+ are governed by the same scaling laws as for similar-size spherical high-viscosity droplets or solid particles [2, 16], i.e.

$$\frac{\mathcal{U}_{max} - U_x}{\mathcal{U}} \sim \left(\frac{a}{\ell_z}\right)^2 \tag{7}$$

where $\mathcal{U}_{max}/\mathcal{U} \approx 2.096$ is the maximum undisturbed velocity at the centerline of a square channel with half-height ℓ_z and average velocity $\mathcal{U}$, and

$$\frac{\Delta P^+}{\Pi} \sim \left(\frac{a}{\ell_z}\right)^5 \tag{8}$$

Both equations represent well the capsule properties at the upstream square channel studied in this work, as shown in figure 3 for capsule centroid $x_c/\ell_z < -2.5$, if we consider that for that channel its half-height is $1.5\ell_z$ and the average velocity is $4/9\mathcal{U}$.

In addition, our earlier investigation [19] revealed that for thick capsules with size $0.8 \lesssim a/\ell_z \leq 1.3$, the confined bullet-like capsules also follow the dynamics of high-viscosity droplets of similar shape, but now the velocity and additional pressure drop are affected by the film thickness h between the capsule membrane and the solid walls,

$$\frac{U_x - \mathcal{U}}{\mathcal{U}} \sim \frac{h}{\ell_z} \tag{9}$$

$$\frac{\Delta P^+}{\Pi} \sim \left(\frac{a}{\ell_z}\right)^2 \frac{a}{h} \tag{10}$$

where the thickness h depends on both the capillary number and the (growing) membrane tensions. The monotonic decrease of the capsule velocity U_x and the significant increase of the additional pressure drop ΔP^+ with the size a/ℓ_z for thick capsules (owing to the associated decrease of the film thickness h) are clearly shown in figure 3 for $x_c/\ell_z \geq 1$.

Our results presented in figure 3 reveal that the converging constriction achieves a monotonic connection of the small- and large-capsule regimes for the capsule velocity and additional pressure difference. Therefore, our interest is now focused on the non-trivial deformation overshooting occurring as the capsule moves out of the constriction and into the smaller square channel at the right, shown earlier in figure 2(c). This transient capsule elongation results in a maximum length L_x and a minimum height L_z of the capsule as seen in figure 4. (These lengths are determined as the maximum distance of the capsule's interface in the x and z directions.) We emphasize that the overshooting of the capsule length L_x is significant for all capsule sizes studied while our larger capsules with $a/\ell_z \geq 1.2$ need more time traveling in the downstream square channel to obtain their steady-state bullet-like shape.

4. SHEAR MODULUS DETERMINATION

In this section, we investigate in detail the transient deformation overshooting occurring as the capsule moves out of the constriction and into the smaller downstream square channel. In particular, we identify its dependence on all the problem parameters, including flow properties (capillary number Ca and viscosity ratio λ) and membrane properties (hardness C and prestress).

Figure 5 shows that the deformation overshooting is more pronounced as the flow rate Ca increases for a given capsule, owing to the stronger deforming hydrodynamics forces. Clearly, the constriction's cross-sectional

area decrease over a relatively short length ℓ_{con} results in strong hydrodynamic forces which overcome locally the weak restoring membrane tensions and produce a transient maximum capsule elongation. As seen in figure 5(a), the overshooting in the capsule length L_x is significant, and thus measurable, and can be used to determine the membrane's shear modulus G_s, as discussed in this section.

Figure 6 reveals that the capsule's elongation overshooting does not depend on the fluids viscosity ratio for low and moderate values, $\lambda \leq 1$. We emphasize that, in general, the transient capsule deformation under external flow changes shows three viscosity-ratio regimes owing to the combined effects of the surrounding and inner fluids' normal stresses on the capsule interface [27]. For low enough viscosity ratio, e.g. for $\lambda \leq 0.01$, the inner fluid does not practically participate in the transient dynamics, and thus all low-viscosity capsules show identical evolution. For moderate viscosity ratios, $\lambda = O(1)$, both the inner and the surrounding fluids' normal stresses affect the capsule deformation. For very viscous capsules (e.g. $\lambda \geq 5$), it is the inner fluid which mostly affects the capsule deformation. In this case, as the viscosity ratio λ increases, the time necessary for the capsule to react to the flow changes imposed by the constriction [27]

$$t_m \sim (1+\lambda)\,\mathrm{Ca}\,\frac{a}{\ell_z}\,t_f \tag{11}$$

(where $t_f = \ell_z/\mathcal{U}$ is the flow time scale) is increased significantly, and thus the capsule deformation rate is slower resulting in a decrease of the capsule's transient deformation, as seen in figure 6 for $\lambda = 10$. The important contribution of the converging constriction used in the present study is that it makes the capsule's elongation overshooting practically independent of the viscosity ratio λ for *both* low and moderate values, i.e. for $\lambda \leq 1$, as seen in figure 6. In particular, our results for both capsule sizes studied ($a/\ell_z = 1, 1.2$) show that the relative difference in the maximum capsule length L_x^{max} of the transient overshooting is less than 0.5% for $\lambda \leq 1$ and becomes much smaller (i.e. less than 0.05%) for $\lambda \leq 0.1$.

Figure 7 reveals a very important feature of the capsule's elongation overshooting, that for the parameter space studied, it does not depend on the membrane hardness C, and thus on the membrane's area-dilatation modulus G_a. Therefore, this transient elongation overshooting is characterized by only shape-changing (i.e. elongation) of the characteristic membrane elements but under constant local surface area. Observe that the capsule's steady-state bullet shape in the downstream square channel does depend weakly on the membrane hardness C, as shown in figure 7 for capsule centroid $x_c/\ell_z \geq 2$.

To investigate further this feature, we studied the dynamics of capsules with sizes $a/\ell_z = 1, 1.2$ at the characteristic flow rate $\mathrm{Ca} = 0.05$, for different membrane harnesses C. In particular, we studied capsules with membrane hardness $C = 0.1, 0.3, 0.5, 1, 2, 5$ and the same initial prestress tension τ_0, namely $\tau_0/G_s \approx 0.1597, 0.3401, 0.5432, 0.7716$. (These values of τ_0 correspond to the prestress parameter $\alpha_p = 0.025, 0.05, 0.075, 0.1$ for a capsule with $C = 1$.) Our results for both capsule sizes studied ($a/\ell_z = 1, 1.2$) show that the relative difference in the maximum capsule length L_x^{max} of the transient overshooting for different membrane harnesses C and the same prestress τ_0 is much less than 1% for the three largest prestress tensions τ_0, and becomes less than 2% for the smallest τ_0 studied, i.e. for $\tau_0/G_s \approx 0.1597$. In essence, for the parameter space studied in this work, the capsule's elongation overshooting is practically independent of the membrane hardness C, and thus of the membrane's area-dilatation modulus G_a.

Figure 8 shows the effects of the capsule prestress on the transient interfacial deformation. For a given flow rate Ca (i.e. given deforming hydrodynamic forces), the capsule deformation is decreased as the capsule prestress increases, owing to the fact that the capsule's prestress τ_0 contributes to the restoring membrane tensions.

The capsule's elongation overshooting owing to the converging constriction is shown in figure 9 as a function of the capillary number Ca for different initial prestress tensions τ_0 and for a given capsule size ($a/\ell_z = 1$). We emphasize that our results shown in this figure, which are formally valid for $\lambda = 1$ and $C = 1$, in reality represent low and moderate viscosity ratios, $\lambda \leq 1$, and a wide range of membrane hardness C (e.g. at least $C = 0.1$–5), since for this parameter space, low or moderate viscosity ratios λ and the membrane hardness do not practically affect the capsule's overshooting.

Our investigation of the capsule's transient length overshooting has revealed a new method to identify a membrane's shear modulus G_s, independently of its area-dilatation modulus G_a, by flowing the capsule in the proposed converging constriction of comparable size, i.e. $a/\ell_z = O(1)$, and compare the experimental measurements of the capsule elongation overshooting L_x^{max} with computation data.

To explain in detail the new method for the shear modulus determination, we propose to flow strain-hardening capsules of a given size a in the converging constriction under Stokes flow conditions, utilize surrounding fluids with known viscosities μ and known average undisturbed velocities $\mathcal{U}$, and measure the capsule maximum length L_x^{max} (e.g. via a high-speed camera). Figure 9 shows that by utilizing relatively low flow rates, $\mathrm{Ca} = 0.02$–0.2, the effects of the capsule prestress τ_0 on the length overshooting are significant, and thus capsules with different prestress τ_0 can easily be distinguished. Note that low flow rates are easy to accomplished since they do not result in membrane rupture [18, 22, 23].

Our proposed method involves the experimental measurement of the elongation overshooting L_x^{max} of a capsule (or an array of similar capsules) with a given prestress τ_0 at several low flow rates. Matching of the experimental measurements with computational data, like those shown in figure 9, should reveal both the capsule's

prestress τ_0 and the capillary number $\mathrm{Ca} = \mu\mathcal{U}/G_s$, i.e. the membrane's shear modulus G_s. Since the length overshooting does not depend practically on the membrane hardness C, our methodology determines the membrane's shear modulus G_s without the need to know the area-dilatation modulus G_a or the moduli ratio G_a/G_s.

We emphasize that our results are independent of the exact shape of the converging constriction since we derived very similar (or practically identical) results utilizing other converging shapes, including "half-cosine" and "straight-line" connections, given by Eqs.(2) and (3) in section 2. As seen in figure 10, while the different constriction shapes produce a small shift in the deformation evolution with respect to the capsule centroid x_c, the length overshooting L_x^{max} is identical for all three constriction shapes.

5. DESIGN OF THE EXPERIMENTAL APPARATUS

In this section, we discuss the requirements for the actual utilization of the proposed experimental device. Our methodology involves flowing strain-hardening capsules in a converging micro-capillary of comparable size, under Stokes flow conditions with capillary number $\mathrm{Ca} = O(0.1)$, and comparing the experimental measurements of the capsule elongation overshooting with computation data.

(i) The requirement of low Reynolds number in the surrounding fluid is commonly achieved by employing high-viscosity surrounding fluids such as concentrated aqueous solutions of glycerin, Pale oils or silicon fluids [4, 18, 22, 23]. (The Reynolds number of the capsule fluid is irrelevant since, during both the steady-state motion in the square channels and the transient deformation in the constriction, the capsule translates as a solid-like particle with zero or very small inner circulation [19, 27].)

For example, we can utilize micro-channels with half-size $\ell_z = 25\,\mu$m to study similar-size micro-capsules made from a cross-linked ovalbumin membrane which have a shear modulus $G_s \approx 0.04\,$N/m [18]. To achieve capillary numbers $\mathrm{Ca} = O(0.1)$, viscous stresses $\mu\mathcal{U} = \mathrm{Ca}\,G_s = 4 \times 10^{-3}$ N/m need to be applied. Utilizing (nearly) 100% solutions of glycerin (with viscosity $\mu \approx 1\,$Pa s and density $\rho \approx 10^3\,\mathrm{kg/m^3}$), the average velocity should be $\mathcal{U} = 4\,$mm/s and thus the external Reynolds number is $\mathrm{Re} = \rho\mathcal{U}\,\ell_z/\mu = 10^{-4}$.

(ii) To measure the capsule's maximum length L_x^{max}, a high-speed camera (combined with a magnification microscope) should be utilized with a center at the beginning of the constriction, i.e. at $x/\ell_z = -1$. The camera view should cover the entire capsule during the elongation overshooting but it is helpful to also cover the channel upstream of the constriction, i.e. the camera should cover the channel length $[-5\ell_z, 3\ell_z]$. Our computational results shown in figures 4–8 reveal that that capsule's maximum length practically occurs (i.e. with an error of 1%) during a period corresponding to the constriction's half-length, $\Delta x = \ell_{con}/2 = \ell_z/2$. Combining this with typical capsule velocities under Stokes flow conditions and capillary number $\mathrm{Ca} = O(0.1)$, we can easily determine the camera's recording speed.

For example, for the ovalbumin micro-capsules discussed in (i) above, the capsule's maximum length practically occurs during a time period $\Delta t = \Delta x/\mathcal{U} = 12.5\,\mu\mathrm{m}/(4\,\mathrm{mm/s}) \approx 3 \times 10^{-3}$ s, and thus a high-speed camera of 1000 frames per second (FPS) is sufficient to record the elongation overshooting. Higher FPS (such as 2000 or 4000) can produce more images of the capsule inside the constriction (and thus serve as verification that the capsule has achieved its maximum length), but it is not necessary. These recording speeds are available in cameras with resolution of at least 960 pixels per direction (as the Phantom v9.1 camera). Therefore, the channel view of $[-5\ell_z, 3\ell_z]$ has a calibration scale of $8 \times 25\,\mu\mathrm{m}/(960\,\mathrm{pixels}) = 0.21\,\mu$m/pixel and thus the capsule dimensions, L_x and L_z, can be measured with an error much less than 1%.

We emphasize that the FPS requirement of the recording camera is not as high as if one wants to record the evolution of the capsule length as a function of time, since here we are only interested in measuring the capsule's maximum length L_x^{max}, which practically occurs during a length $\Delta x = \ell_z/2$. In essence, our camera requirement is very similar to that for steady-state capsule motion in micro-ducts. For example, for the ovalbumin micro-capsules discussed here, Hu *et al.*[18] utilized straight microfluidic channels of similar size as the one proposed in this work, and employed a 1000 frames-per-second camera to record the steady-steady capsule motion.

(iii) The size of the capsule a can be determined from the same micro-device by measuring the capsule height L_z in the upstream square channel. (Observe that, owing to the channel's larger size, the capsule height L_z is practically equal to its undisturbed diameter $2a$ as seen in figures 4(b) and 5(b).) Thus, by utilizing the camera view $[-5\ell_z, 3\ell_z]$, the capsule size a can be determined very accurately (with an error of less than 1%).

(iv) Owing to the continuous flow in the micro-capillary, it is possible the characterization of a large number of artificial capsules with similar properties. In this case, utilizing dilute suspensions of capsules we can easily guarantee that the distance between successive capsules is sufficient large (i.e. more than 20–50 times the capsule size a) to produce negligible interactions between neighboring capsules under Stokes flow conditions [40]. In addition, since our methodology involves spherical capsules with comparable size with that of the micro-capillary, the capsules are expected to have been aligned with the micro-capillary centerline during their motion in the area further upstream the constriction [19].

(v) Our methodology assumes homogeneity of the membrane's material and thickness, as most existing techniques do. This homogeneity is an actual goal during the capsule fabrication and can be achieved via efficient

mixing of the cross-linking agent, e.g. via capsule motion in a wavy micro-channel [8, 37]. In addition, our computational investigation considers the membrane as a two-dimensional continuum with shearing and area-dilatation resistance but negligible bending resistance. This modeling has been proven to be an excellent description of a wide range of thin elastic membranes (up to a membrane thickness of 5% the capsule size) [3, 10, 11, 23, 28].

It is of interest to note that the shear modulus G_s has been found to increase with the membrane thickness [24]. Capsules with different membrane thickness can be fabricated by using different concentrations of the cross-link agents [24]. Thus, we can identify the effects of the membrane thickness on the shear modulus by performing different experiments with the proposed device for capsules fabricated with different concentrations of the cross-link agents.

(vi) Our results included in this paper involve spherical capsules which are commonly fabricated via interfacial polymerization of liquid droplets [8, 14, 26]. Since this process may also produce a (small) number of nearly-spherical capsules, it is interesting to mention that the properties of our proposed methodology are also valid for such capsules, as our computational results for nearly-spherical prolate and oblate capsules reveal.

(vii) Having considered the details of the experimental apparatus, we discuss now how the measurement error in the relevant variables (L_x^{max}, a, μ, $\mathcal{U}$) affect the determination of the membrane's shear modulus G_s. Figure 9 shows that the scaled length overshooting $L_x^{max}/(2a)-1$ is sub-linearly proportional to the capillary number $\mathrm{Ca} = \mu\mathcal{U}/G_s$, and thus the greater contribution in the G_s error results from the measurement error in the capsule's maximum length L_x^{max}. To find this contribution, in figure 11 we replot the data shown earlier in figure 9, but now the scaled length overshooting $L_x^{max}/(2a) - 1$ is plotted as a function of the inverse capillary number $\mathrm{Ca}^{-1} = G_s/(\mu\mathcal{U})$. The bold curve shows the data for a capsule with $C = 1$ and prestress $\alpha_p = 0.05$ but with +1% error in the capsule length L_x^{max}, i.e. we use $1.01\,L_x^{max}$ to plot the data in this case.

By measuring the differences caused by the +1% error in the capsule length shown in figure 11, we found that for a typical length overshooting $L_x^{max}/(2a) - 1$ of 0.2–0.3, 1% error in the capsule length L_x^{max} creates 7% error in the measured shear modulus G_s. The error in G_s increases to 10% for a length overshooting of 0.1. In addition, our results show that 2% error in the capsule length L_x^{max} doubles the aforementioned errors in the measured shear modulus. On the other hand, the capsule size a does not contribute any significant error in G_s owing to its accurate determination as described in (iii) above. In addition, a small error in the measurement of the viscosity μ of the surrounding fluid or the average velocity $\mathcal{U}$ creates only a comparable (i.e. small) error in the measured shear modulus. Such small errors are contain within the larger error caused by the measurement of the capsule length L_x^{max}. We emphasize that the errors reported here are further reduced (via division with the square root of the number of measurements at different flow rates) in determining the standard deviation of the mean which is usually reported in experimental measurements.

Thus, the error in determining a membrane's shear modulus G_s via our methodology is comparable to that of existing modulus methodologies which reported a relative standard deviation of 15–30% in the mean G_s value for an array of similar capsules. (See for example, the variation in the shear modulus determination included in tables 2 and 3 in Ref.[21], in figures 6 and 7 in Ref.[8], and in figure 10 in Ref.[18].) Furthermore, for methodologies which assumed a value of the moduli ratio G_a/G_s, there may exist an additional error in the G_s determination resulting from this assumption.

We conclude this section by emphasizing that for an accurate determination of the shear modulus, it is important that the capsule deformation is known precisely. To achieve this goal, accurate modulus methodologies do not rely on approximate relationships (e.g. approximate analytical models or fitting laws for computational results) to express the capsule deformation. Instead, they compare the experimental measurements with actual computational results in the same device or exact analytical relationships [8, 18, 24], as we also propose for our methodology. (Observe that an approximate relationship for the capsule length, with an error of 5% or higher, creates a really significant error in the G_s determination as can be deduced from figure 11.)

6. CONCLUSIONS

The determination of the elastic properties of the membrane of artificial capsules (i.e. the shear modulus G_s and area-dilatation modulus G_a) is essential for the better design of the various devices that are utilized in their engineering and biomedical applications. However, such determination is a challenging task, while two experimental techniques are commonly required to account for the combined effects of the shear and area-dilatation moduli on the membrane deformation, as well as significant testing to verify the correct value of the moduli ratio G_a/G_s. This task is more complicated for experimental techniques involving three-dimensional capsule deformation (e.g. flow in microfluidic channels) since the required for comparison three-dimensional computational data may be difficult to obtain for a wide rage of G_a/G_s.

Based on computational investigation, in this study we have developed a new methodology to determine a membrane's shear modulus G_s, independently of its area-dilatation modulus G_a, by flowing strain-hardening capsules in a converging micro-capillary of comparable size under Stokes flow conditions, and comparing the experimental measurements of the capsule elongation overshooting with computation data. This methodology relies on an important feature of the capsule motion from a

larger axisymmetric-like channel to a smaller channel via a converging connection. Namely, that, as the capsule enters the smaller channel, the elongation overshooting does not depend practically on the membrane's modulus ratio G_a/G_s and thus on the membrane's area-dilatation modulus G_a. Therefore, this transient elongation overshooting is characterized by only shape-changing (i.e. elongation) of the characteristic membrane elements but under constant local surface area. Furthermore, we found that the effects of the capsule prestress on the length overshooting are significant, and thus capsules with different prestress can easily be distinguished via the comparison of experimental and computational findings. After the shear modulus determination, the area-dilatation modulus G_a of the membrane can easily be determined via any existing methodology, e.g. steady-state motion in a micro-channel.

The elongation overshooting is practically independent of the viscosity ratio for low and moderate viscosity ratios, and thus a wide range of capsule fluids can be employed. In addition, our methodology involves low flow rates (which are easy to accomplished since they do not result in membrane rupture) while it does not depend on the exact shape or length of the converging connection between the two micro-channels. Our proposed experimental device can be readily produced via glass fabrication while owing to the continuous flow in the microcapillary, it is possible the characterization of a large number of artificial capsules of similar properties. The requirements for the actual utilization of our experimental device are very similar to those of existing experimental techniques for shear modulus determination employing micro-channels or micro-capillaries [18, 22, 23]. To the best of our knowledge, this is the first methodology which can determine a membrane's shear modulus independently of its area-dilatation modulus for an array of capsules.

It is of interest to note that a wide range of methodologies have been developed for the determination of the shear modulus G_s of the erythrocyte membrane, utilizing micro-pipette aspirations, optical tweezers, ektacytometry systems and flow in micro-channels, e.g. [15, 17, 25, 38]. Although similar, the erythrocyte methodologies also show important differences compared to those for artificial capsules. In particular, erythrocyte methodologies usually treat the cell membrane as locally area-incompressible, and thus they seek to find the shear modulus G_s without considering area-dilatation effects. Most important, owing to inherent differences in a population of erythrocytes, the complexity of the cell membrane, and the development of physically different erythrocyte modelings over several decades, very large variations on the determination of the erythrocyte's shear modulus G_s (in the range of $[1-10]$ μN/m) are considered acceptable [9, 15, 17, 25]. (In essence, physiological membranes introduce additional challenges for their characterization.) In contrast, for artificial capsules both moduli, G_s and G_a, affect (in general) the interfacial deformation and thus the moduli determination, while a more accurate moduli determination is sought and achieved, as we discuss at the end of section 5.

ACKNOWLEDGMENTS

This work was supported in part by the National Science Foundation. Most computations were performed on multiprocessor computers provided by the Extreme Science and Engineering Discovery Environment (XSEDE) which is supported by the National Science Foundation.

[1] M. Abkarian, M. Faivre, R. Horton, K. Smistrup, C. A. Best-Popescu and H. A. Stone, Cellular-scale hydrodynamics. *Biomed. Mater.* **3**, 034011(1-13) (2008).

[2] H. Brenner, Pressure drop due to the motion of neutrally buoyant particles in duct flows. II. Spherical droplets and bubbles. *Ind. Engng Chem. Fundam.* **10**, 537–543 (1971).

[3] M. Carin, D. Barthès-Biesel, F. Edwards-Lévy, C. Postel, and D. C. Andrei, Compression of biocompatible liquid-filled HSA-alginate capsules: determination of the membrane mechanical properties. *Biotech. Bioeng.* **82**, 207–212 (2003).

[4] K. S. Chang and W. L. Olbricht Experimental studies of the deformation of a synthetic capsule in extensional flow. *J. Fluid Mech.* **250**, 587–608 (1993).

[5] K. S. Chang and W. L. Olbricht Experimental studies of the deformation and breakup of a synthetic capsule in steady and unsteady simple shear flow. *J. Fluid Mech.* **250**, 609–633 (1993).

[6] M. Chabert and J.-L. Viovy Microfluidic high-throughput encapsulation and hydrodynamic self-sorting of single cells. *Proc. Natl. Acad. Sci.* **105**, 3191–3196 (2008).

[7] W. Chen, Y. Yang, C. Rinadi, D. Zhou and A. Q. Shen, Formation of supramolecular hydrogel microspheres via microfluidics. *Lab Chip* **9**, 2947–2951 (2009).

[8] T. X. Chu, A.-V. Salsac, D. Barthès-Biesel, L. Griscom, F. Edwards-Lévy and E. Leclerc, Fabrication and in situ characterization of microcapsules in a microfluidic system. *Microfluid Nanofluid* **14** 309–317 (2013).

[9] P. Dimitrakopoulos, Analysis of the variation in the determination of the shear modulus of the erythrocyte membrane: Effects of the constitutive law and membrane modeling. *Phys. Rev. E.* **85** 041917 (2012).

[10] P. Dimitrakopoulos, Effects of membrane hardness and scaling analysis for capsules in planar extensional flows. *J. Fluid Mech.* **745**, 487–508 (2014).

[11] W. R. Dodson III and P. Dimitrakopoulos, Tank-treading of erythrocytes in strong shear flows via a non-stiff cytoskeleton-based continuum computational modeling. *Biophys. J.* **99**, 2906–2916 (2010).

[12] W. R. Dodson III and P. Dimitrakopoulos, Dynamics of strain-hardening and strain-softening capsules in strong planar extensional flows via an interfacial spectral boundary element algorithm for elastic membranes. *J. Fluid Mech.* **641**, 263–296 (2009).

[13] W. R. Dodson III and P. Dimitrakopoulos, Properties of the spindle-to-cusp transition in extensional capsule dynamics. *Europhys. Lett.* **106** 48003 (2014).

[14] W. J. Duncanson, T. Lin, A. R. Abate, S. Seiffert, R. K. Shah and D. A. Weitz, Microfluidic synthesis of advanced microparticles for encapsulation and controlled release. *Lab Chip* **12**, 2135–2145 (2012).

[15] S. Hénon, G. Lenormand, A. Richert, and F. Gallet, A new determination of the shear modulus of the human erythrocyte membrane using optical tweezers. *Biophys. J.* **76**, 1145–1151 (1999).

[16] G. Hetsroni, S. Haber and E. Wacholder, The flow in and around a droplet moving axially within a tube. *J. Fluid Mech.* **41**, 699–705 (1970).

[17] R. M. Hochmuth, and R. E. Waugh, Erythrocyte membrane elasticity and viscosity. *Annu. Rev. Physiol.* **49**, 209–219 (1987).

[18] X.-Q. Hu, B. Sévénié, A. V. Salsac, E. Leclerc and D. Barthès-Biesel, Characterizing the membrane properties of capsules flowing in a square-section microfluidic channel: Effects of the membrane constitutive law. *Phys. Rev. E* **87**, 063008 (2013).

[19] S. Kuriakose and P. Dimitrakopoulos, Motion of an elastic capsule in a square microfluidic channel. *Phys. Rev. E.* **84** 011906 (2011).

[20] S. Kuriakose and P. Dimitrakopoulos, Deformation of an elastic capsule in a rectangular microfluidic channel. *Soft Matter*, **9** 4284–4296 (2013).

[21] I. Koleva and H. Rehage, A comparison of different experimental methods for investigating the mechanical properties of plane polysiloxane membranes and capsule walls. *Soft Matter* **8**, 7672–7682 (2012).

[22] E. Leclerc, H. Kinoshita, T. Fujii and D. Barthès-Biesel, Transient flow of microcapsules through convergent-divergent microchannels. *Microfluid Nanofluid* **12**, 761–770 (2012).

[23] Y. Lefebvre, E. Leclerc, D. Barthès-Biesel, J. Walter and F. Edwards-Lévy, Flow of artificial microcapsules in microfluidic channels: A method for determining the elastic properties of the membrane. *Phys. Fluids* **20**, 123102 (2008).

[24] C. de Loubens, J. Deschamps, M. Georgelin, A. Charrier, F. Edwards-Levy and M. Leonetti, Mechanical characterization of cross-linked serum albumin microcapsules. *Soft Matter* **10**, 4561–4568 (2014).

[25] J. P. Mills, L. Qie, M. Dao, C. T. Lim, and S. Suresh, Nonlinear elastic and viscoelastic deformation of the human red blood cell with optical tweezers. *Mech. Chem. Biosys.* **1**, 169–180 (2004).

[26] M. P. Neubauer, M. Poehlmann, A. Fery. Microcapsule mechanics: From stability to function. *Advances in Colloid and Interface Science* **207** 65–80 (2014).

[27] S.-Y. Park and P. Dimitrakopoulos Transient dynamics of an elastic capsule in a microfluidic constriction. *Soft Matter* **9**, 8844–8855 (2013).

[28] G. Pieper, H. Rehage, and D. Barthès-Biesel, Deformation of a capsule in a spinning drop apparatus. *J. Colloid Interface Sci.* **202**, 293–300 (1998).

[29] C. Pozrikidis (ed.), *Modeling and Simulation of Capsules and Biological Cells*. Chapman and Hall, London (2003).

[30] M. Prevot, A. L. Cordeiro, G. B. Sukhorukov, Y. Lvov, R. S. Besser, and H. Möhwald, Design of a microfluidic system to investigate the mechanical properties of layer-by-layer fabricated capsules. *Macromol. Mater. Eng.* **288**, 915–919 (2003).

[31] D. J. Quinn, I. Pivkin, S. Y. Wong, K.-H. Chiam, M. Dao, G. E. Karniadakis, and S. Suresh, Combined simulation and experimental study of large deformation of red blood cells in microfluidic systems. *Ann. Biomed. Eng.* **39**, 1041-1050 (2011).

[32] F. Risso, F. Collé-Pailot and M. Zagzoule, Experimental investigation of a bioartificial capsule flowing in a narrow tube. *J. Fluid Mech.* **547**, 149–173 (2006).

[33] S. Seiffert, J. Thiele, A. R. Abate and D. A. Weitz, Smart microgel capsules from macromolecular precursors. *J. Am. Chem. Soc.* **132**, 6606–6609 (2010).

[34] A. S. Utada, E. Lorenceau, D. R. Link, P. D. Kaplan, H. A. Stone and D. A. Weitz, Monodisperse double emulsions generated from a microcapillary device. *Science* **308**, 537–541 (2005).

[35] H. M. Wyss, T. Franke, E. Melead and D. A. Weitz, Capillary micromechanics: measuring the elasticity of microscopic soft objects. *Soft Matter* **6**, 4550–4555 (2010).

[36] R. Skalak, A. Tozeren, R. P. Zarda, and S. Chien, Strain energy function of red blood cell membranes. *Biophys. J.* **13**, 245–264 (1973).

[37] S.-Y. Teh, R. Lin, L.-H. Hung and A. P. Lee, Droplet microfluidics. *Lab Chip* **8**, 198–220 (2008).

[38] G. Tomaiuolo, M. Barra, V. Preziosi, A. Cassinese, B. Rotolid, and S. Guido, Microfluidics analysis of red blood cell membrane viscoelasticity. *Lab Chip* **11**, 449-454 (2011).

[39] Y. Wang and P. Dimitrakopoulos, Nature of the hemodynamic forces exerted on vascular endothelial cells or leukocytes adhering to the surface of blood vessels. *Phys. Fluids* **18**, 087107(1-14) (2006).

[40] Y. Wang and P. Dimitrakopoulos, Low-Reynolds-number droplet motion in a square microfluidic channel. *Theor. Comput. Fluid Dyn.* **26**, 361–379 (2012).

[41] C.-X. Zhao, Multiphase flow microfluidics for the production of single or multiple emulsions for drug delivery. *Advanced Drug Delivery Reviews* **65**, 1420–1446 (2013).

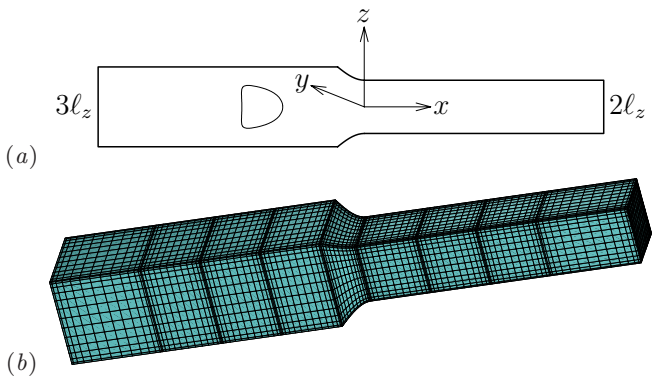

FIG. 1. (a) Illustration of an elastic capsule flowing at the centerline of a converging square micro-channel. (b) Spectral boundary element discretization of the microfluidic geometry.

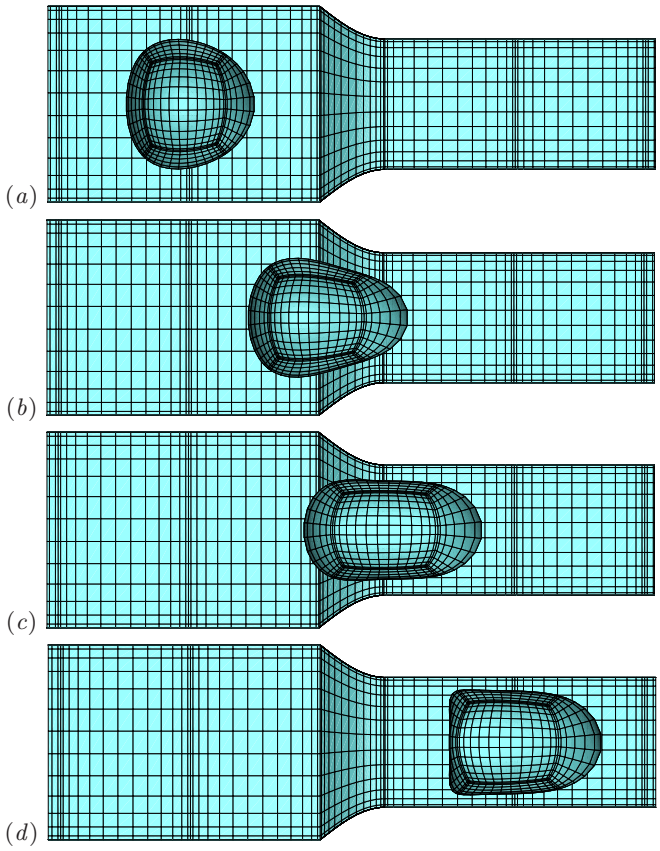

FIG. 2. The shape of a Skalak capsule with $C = 1$, $\alpha_p = 0.05$, $\lambda = 1$, $a/\ell_z = 1$ and Ca $= 0.2$ moving inside the microfluidic geometry. The capsule's centroid x_c/ℓ_z is (a) -3.06, (b) -1.02, (c) 0.07, and (d) 2. The three-dimensional capsule views were derived from the actual spectral grid using orthographic projection in plotting.

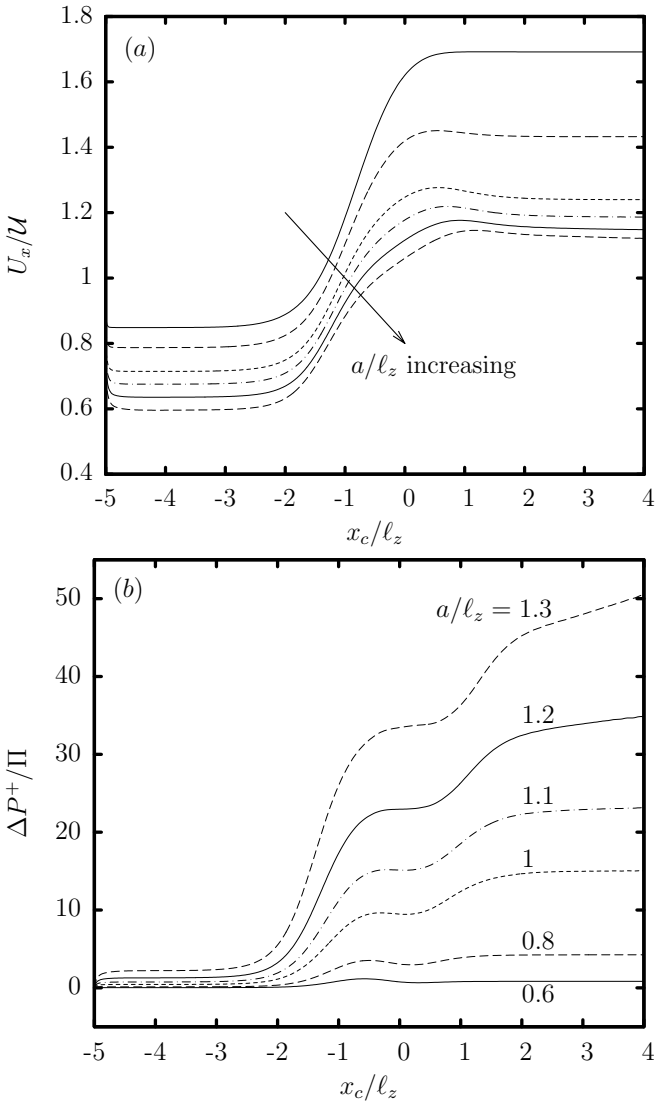

FIG. 3. Evolution of (a) the capsule velocity U_x, and (b) the additional pressure difference ΔP^+, as a function of the centroid x_c, for a Skalak capsule with $C = 1$, $\alpha_p = 0.05$, $\lambda = 1$, Ca $= 0.05$ and size $a/\ell_z = 0.6, 0.8, 0.9, 1, 1.1, 1.2, 1.3$.

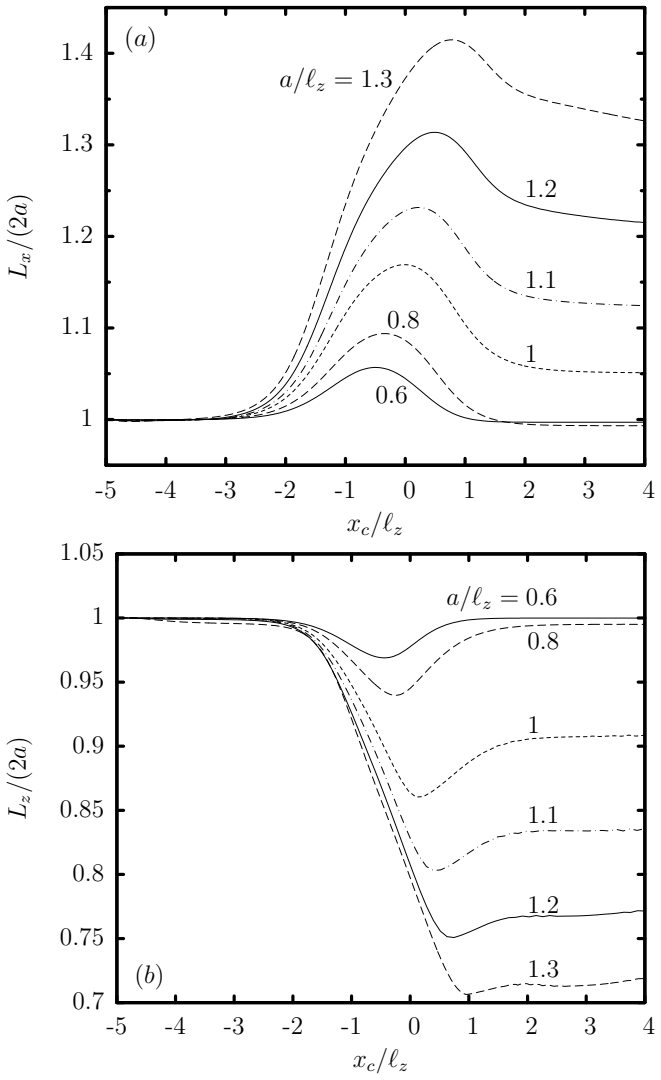

FIG. 4. Evolution of the capsule lengths as a function of the centroid x_c, for a Skalak capsule with $C = 1$, $\alpha_p = 0.05$, $\lambda = 1$, Ca $= 0.05$ and size $a/\ell_z = 0.6, 0.8, 0.9, 1, 1.1, 1.2, 1.3$. (a) Length L_x, and (b) height L_z (scaled with the length $2a$ of the undisturbed spherical shape). These lengths are determined as the maximum distance of the interface in the x and z directions.

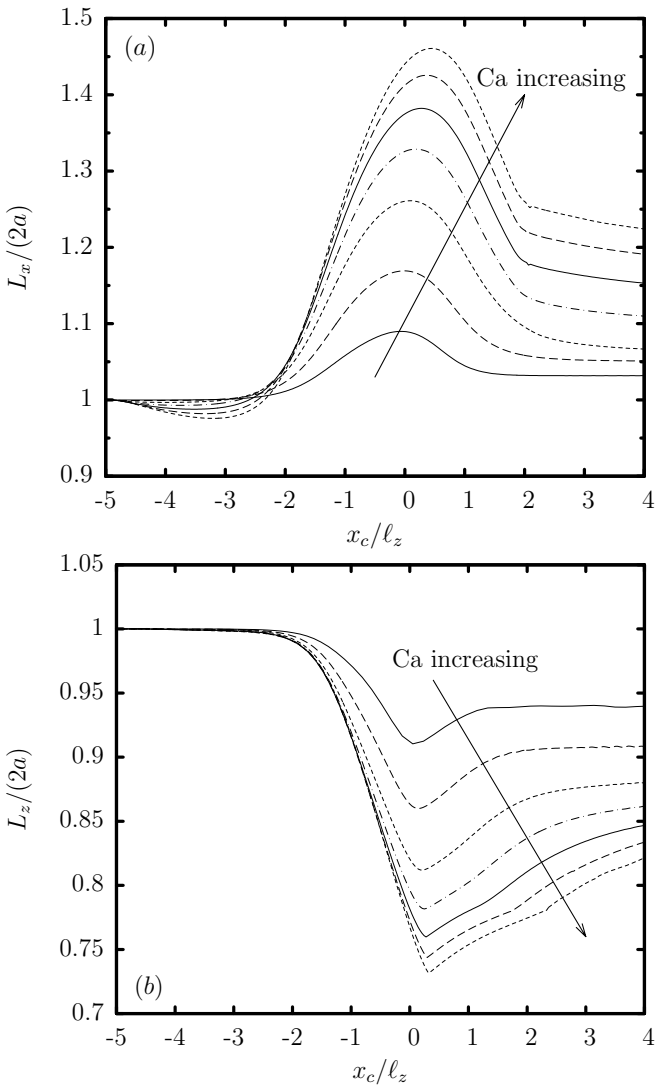

FIG. 5. Evolution of the capsule lengths as a function of the centroid x_c, for a Skalak capsule with $C = 1$, $\alpha_p = 0.05$, $\lambda = 1$, $a/\ell_z = 1$ and capillary number Ca $= 0.02, 0.05, 0.1, 0.15, 0.2, 0.25, 0.3$. (a) Length L_x, and (b) height L_z (scaled with the length $2a$ of the undisturbed spherical shape).

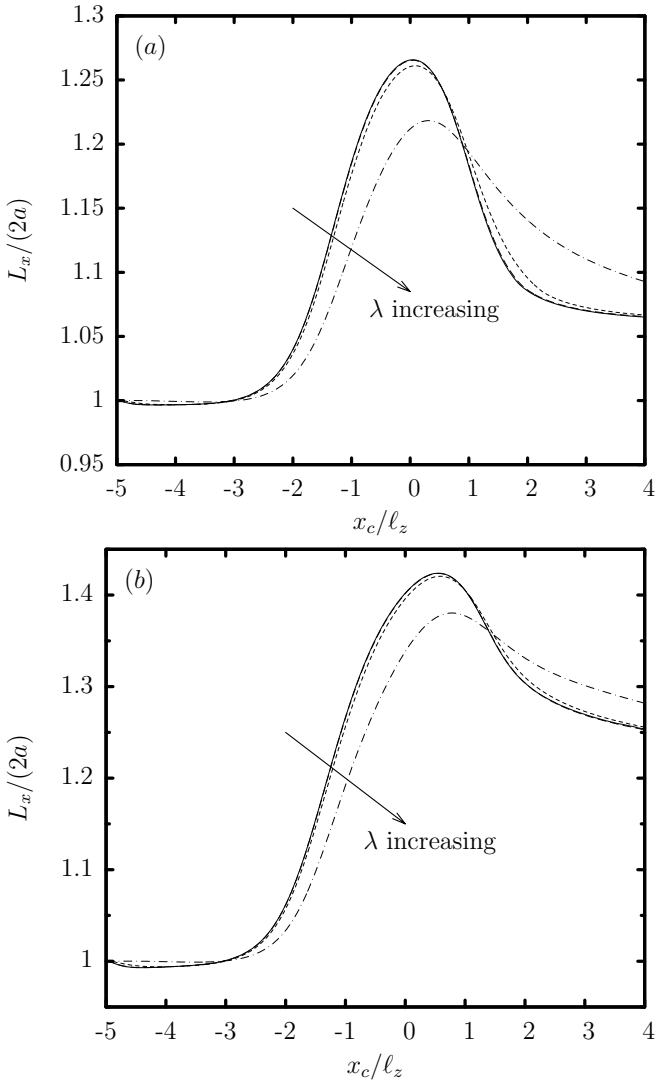

FIG. 6. Evolution of the capsule length L_x as a function of the centroid x_c, for a Skalak capsule with $C = 1$, $\alpha_p = 0.05$, $\mathrm{Ca} = 0.1$ and viscosity ratio $\lambda = 0.01, 0.1, 1, 10$. Capsule size: (a) $a/\ell_z = 1$, and (b) $a/\ell_z = 1.2$. In both cases, the results for $\lambda = 0.1$ are identical to those for $\lambda = 0.01$.

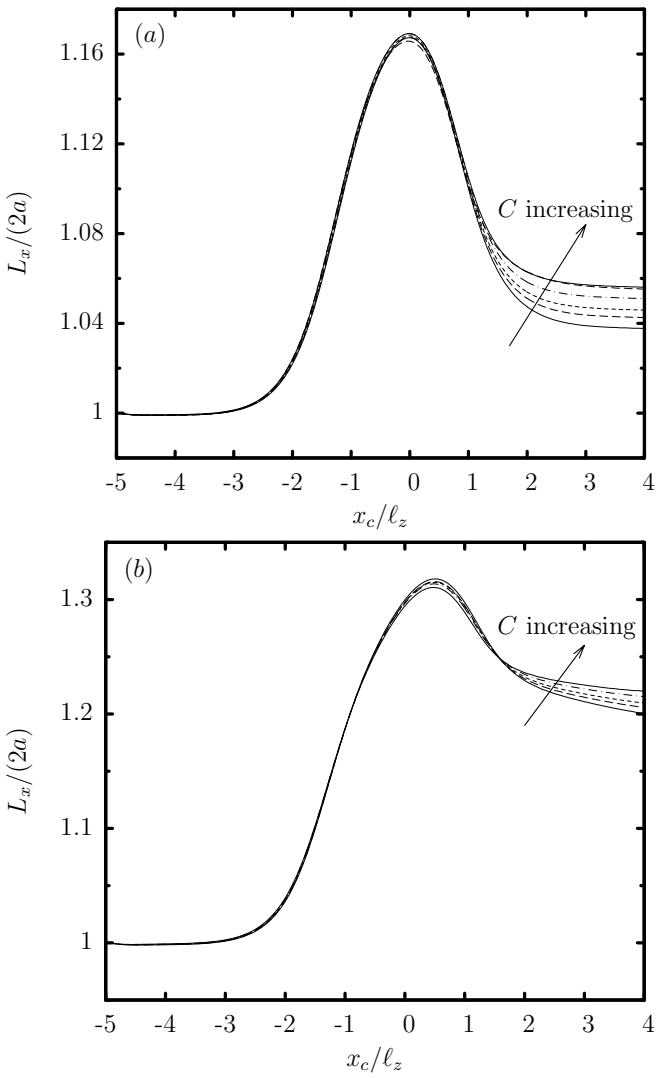

FIG. 7. Evolution of the capsule length L_x as a function of the centroid x_c, for a Skalak capsule with $\lambda = 1$ and $\mathrm{Ca} = 0.05$. Capsule size: (a) $a/\ell_z = 1$, and (b) $a/\ell_z = 1.2$. The membrane hardness is $C = 0.1, 0.3, 0.5, 1, 2, 5$ and the prestress parameter $\alpha_p = 0.1244, 0.0912, 0.0732, 0.05, 0.0311, 0.0147$, respectively, so that all capsules have the same initial prestress tension $\tau_0/G_s \approx 0.3401$.

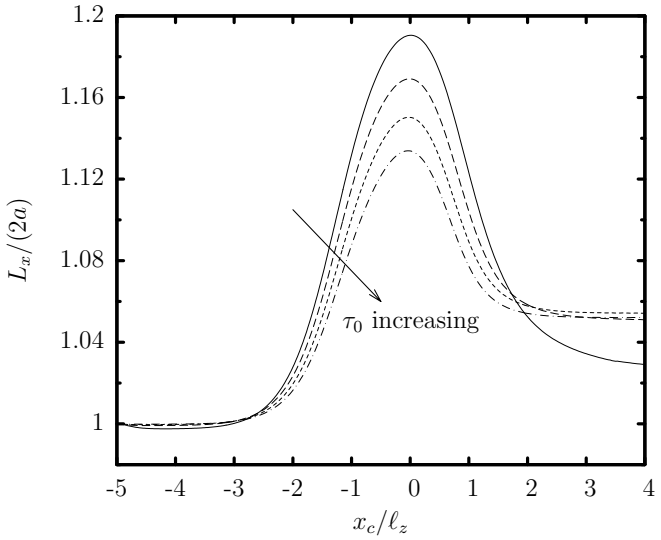

FIG. 8. Evolution of the capsule length L_x as a function of the centroid x_c, for a Skalak capsule with $C = 1$, $\lambda = 1$, $a/\ell_z = 1$ and Ca $= 0.05$. The capsule prestress parameter is $\alpha_p = 0.025, 0.05, 0.075, 0.1$ and thus the initial prestress tension is $\tau_0/G_s \approx 0.1597, 0.3401, 0.5433, 0.7716$, respectively.

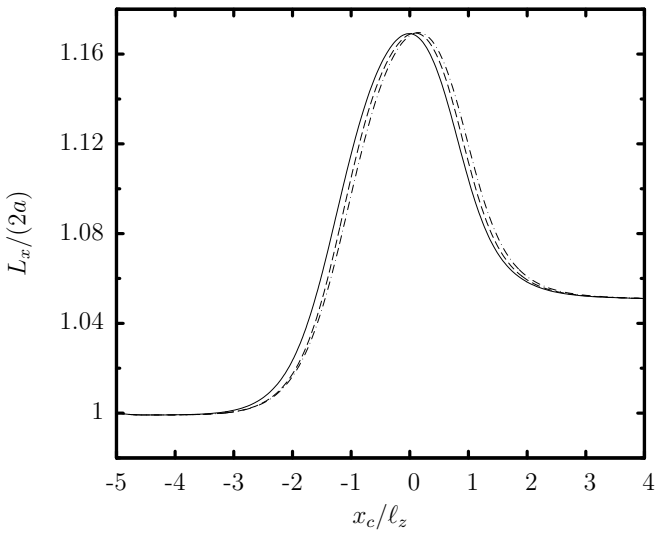

FIG. 10. Evolution of the capsule length L_x as a function of the centroid x_c, for a Skalak capsule with $C = 1$, $\alpha_p = 0.05$, $\lambda = 1$, $a/\ell_z = 1$ and different constriction shapes: ——, "quarter-cosine"; - - -, "half-cosine"; $-\cdot-$, "straight-line".

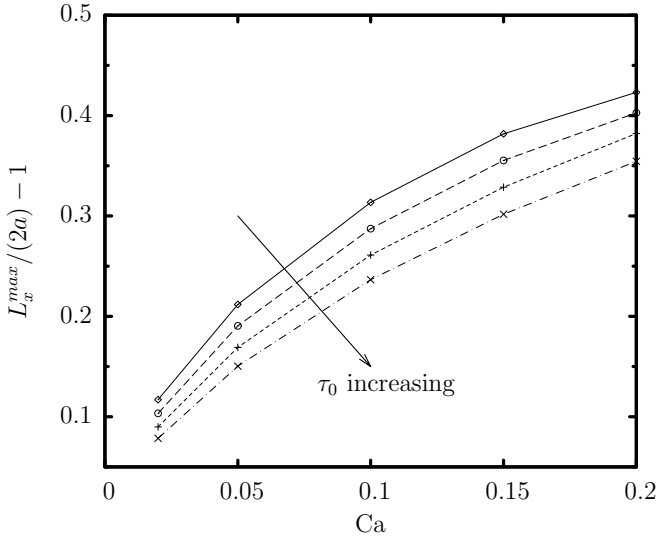

FIG. 9. Scaled length overshooting $L_x^{max}/(2a) - 1$ (where L_x^{max} is the maximum capsule length) as a function of the capillary number Ca, for a Skalak capsule with $C = 1$, $\lambda = 1$, $a/\ell_z = 1$ and capillary number Ca $= 0.02, 0.05, 0.1, 0.15, 0.2$. The initial prestress tension is $\tau_0/G_s \approx 0, 0.1597, 0.3401, 0.5433$ which corresponds to the prestress parameter $\alpha_p = 0, 0.025, 0.05, 0.075$, respectively, for a capsule with $C = 1$. The data for $\alpha_p = 0$ (which cannot be computed via our capsule algorithm due to interfacial breaking) were derived via linear interpolation using the data for $\alpha_p = 0.025, 0.05$.

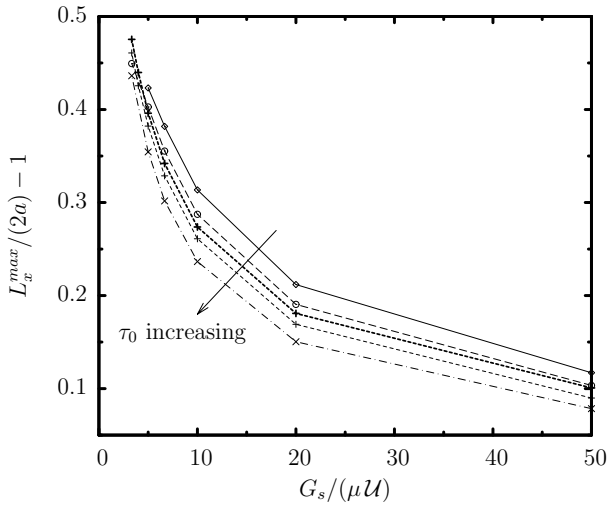

FIG. 11. As in figure 9, but now the scaled length overshooting $L_x^{max}/(2a) - 1$ is plotted as a function of the inverse capillary number $\text{Ca}^{-1} = G_s/(\mu\mathcal{U})$. The bold curve shows the data for a capsule with $C = 1$ and prestress $\alpha_p = 0.05$ but with +1% error in the capsule length L_x^{max}, i.e. we use $1.01\, L_x^{max}$ to plot the data.